

Padé approximation of a stationary single-channel Ca^{2+} nanodomain

Victor Matveev

Department of Mathematical Sciences
New Jersey Institute of Technology
Newark, NJ 07102

Abstract

We consider the stationary solution for the Ca^{2+} concentration near a point Ca^{2+} source describing a single-channel Ca^{2+} nanodomain, in the presence of a single mobile buffer with one-to-one Ca^{2+} binding stoichiometry. Previously, a number of Ca^{2+} nanodomains approximations have been developed, for instance the Excess Buffer approximation (EBA), the Rapid Buffering approximation (RBA), and the Linear approximation (LIN), each valid for appropriate buffering conditions. Apart from providing a simple method of estimating Ca^{2+} and buffer concentrations without resorting to computationally expensive numerical solution of reaction-diffusion equations, such approximations proved useful in revealing the dependence of nanodomain Ca^{2+} distribution on crucial parameters such as buffer mobility and its Ca^{2+} binding properties. Here we present a new form of analytic approximation, which is based on matching the short-range Taylor series of the nanodomain concentration with the long-range asymptotic series expressed in inverse powers of distance from channel location. Namely, we use a “dual” Padé rational function approximation to simultaneously match terms in the short- and the long-range series, and show that this provides an accurate approximation to the nanodomain Ca^{2+} and buffer concentrations. We compare the newly derived method with the previously obtained approximations, and show that it yields a better estimate of the free buffer concentration for a wide range of buffering conditions. The drawback of the presented method is that it has a complex algebraic form for any order higher than the lowest bilinear order, and cannot be readily extended to multiple Ca^{2+} channels. However, it may be possible to extend the Padé method to estimate Ca^{2+} nanodomains in the presence of cooperative Ca^{2+} buffers with two Ca^{2+} binding sites, the case which existing methods do not address.

Keywords: calcium buffer, buffered diffusion, calcium diffusion, calcium modeling, reaction-diffusion

I. Introduction

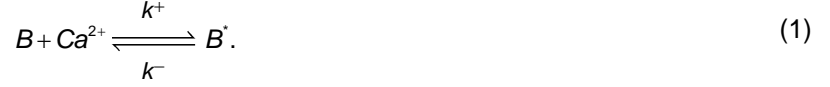
In the face of great diversity of Ca^{2+} -dependent mechanisms, intracellular Ca^{2+} signals have to be localized in time and space to allow selective activation of specific reactions (1-3). This is particularly true in the case of fast Ca^{2+} -triggered processes such as synaptic neurotransmitter release, hormone secretion and muscle contraction, which are controlled by localized Ca^{2+} influx through trans-membrane Ca^{2+} channels (4-7). The tight temporal and spatial localization of Ca^{2+} influx is maintained in part by the abundant intracellular Ca^{2+} buffers that absorb most of the Ca^{2+} influx soon upon its entry through a Ca^{2+} channel (8, 9). The resulting localized Ca^{2+} elevation near a cell membrane Ca^{2+} channel is termed Ca^{2+} *nanodomain*, while corresponding events caused by brief opening of ryanodine and IP3 receptor-coupled Ca^{2+} channels are referred to as *sparks* or *blinks* (2, 7, 10), with relevant spatial scales of 10-100 nm, and the temporal scales of domain formation and collapse on the order of 10-100 μs . It is a great challenge to image Ca^{2+} concentrations on such fine temporal and spatial scales; further, Ca^{2+} -sensitive dyes perturb the very Ca^{2+} signals they are employed to measure. This explains the central role that mathematical modeling of buffered Ca^{2+} diffusion has played in the study of Ca^{2+} dynamics in neurons, endocrine cells and myocytes (2, 3, 11-16)

One of the contributions of early modeling efforts was the development of accurate analytical approximations of quasi-stationary Ca^{2+} nanodomains (15, 17, 18), which estimate the Ca^{2+} and buffer concentration profiles rapidly established near an open Ca^{2+} channel. Such approximations rely on the assumption of simple, one-to-one Ca^{2+} -buffer binding, and can be understood in terms of asymptotic expansions with respect to appropriate model parameters (18) (see Methods). They allow avoiding computationally expensive integration of reaction-diffusion equations or stochastic simulations, while retaining considerable accuracy (19-23). These approximate solutions of deterministic reaction-diffusion equations can be combined with stochastic simulations of channel gating for computational efficiency in modeling cell Ca^{2+} dynamics (20, 24), noting however that buffering may increase Ca^{2+} fluctuations (25), which may in turn influence stochastic gating of Ca^{2+} -dependent Ca^{2+} channels (24, 26). Importantly, approximate closed-form solutions also provide deep insight into the dependence of Ca^{2+} concentration on buffering conditions. For example, the lowest-order Excess Buffer approximation (EBA) yields an approximate Ca^{2+} concentration decay proportional to $\exp(-r/\lambda)/(D_c r)$, where r is the distance from the open Ca^{2+} channel, and the characteristic length $\lambda=[D_c/(k^+/B_T)]^{1/2}$ clearly describes the effect of Ca^{2+} diffusivity D_c , buffer concentration B_T and binding rate k^+ on Ca^{2+} domain localization (15, 18, 27, 28). Also notable is the Rapid Buffering approximation (RBA) (15, 17, 27-30), which has been generalized to an arbitrary collection of Ca^{2+} channels along a flat membrane, despite the nonlinearity inherent in the buffering (21). Finally, the Linear approximation (LIN) is noteworthy for the simplicity of handling an arbitrary number of simple buffers (31), and gives an accurate approximation of Ca^{2+} concentration for a very wide range of buffering conditions (18) (see Fig. 5B, 6).

Despite their great utility, previously developed approximations have several limitations: (i) they lose accuracy and may even yield non-monotonic distance dependence outside of their respective parameter regimes (18), and (ii) they are not easily extended to the case of cooperative buffers with more complex Ca^{2+} binding stoichiometry. Here we present a novel method, which involves matching the low-distance (short-range) and large-distance (long-range) series representations of the single-channel nanodomain solution. We show that the newly developed approximation gives better accuracy in estimating the free buffer concentration within a Ca^{2+} nanodomain, for a broader range of conditions. We believe that it may be possible to extend the new method to complex buffers with two Ca^{2+} binding sites, including buffers such as calmodulin and calretinin that contain EF-hand motifs characterized by cooperative Ca^{2+} binding (32).

II. Materials and Methods

Following previous modeling efforts, we constrain our current analysis to the case of a single dominant Ca^{2+} buffer with molecules possessing a single Ca^{2+} ion binding described by the reaction



Here B and B^* represents the free buffer and Ca^{2+} -bound buffer, respectively (i.e. $B^* = \text{Ca}B$), and k^+ (k^-) are the Ca^{2+} -buffer binding (unbinding) rates. Assuming isotropic diffusion and mass-action kinetics, this yields the following reaction-diffusion system (17, 18)

$$\begin{cases} \text{Calcium:} & \frac{\partial C}{\partial t} = D_C \nabla^2 C - k^+ BC + k^- B^*, \\ \text{Unbound buffer:} & \frac{\partial B}{\partial t} = D_B \nabla^2 B - k^+ BC + k^- B^*, \\ \text{Bound buffer:} & \frac{\partial B^*}{\partial t} = D_B^* \nabla^2 B^* + k^+ BC - k^- B^*. \end{cases} \quad (2)$$

where D_B , D_B^* and D_C are the diffusivities of the free buffer, bound buffer and Ca^{2+} , respectively, and C , B and B^* represents concentrations of Ca^{2+} , free buffer and Ca^{2+} -bound buffer, respectively. The boundary conditions depend on the details of the cellular compartment being modeled, and include at least one point source representing a Ca^{2+} channel. As in prior modeling efforts, we will consider semi-infinite domain bounded by a flat plane, with zero flux boundary condition for Ca^{2+} and buffer. In this case the reflection symmetry allows to extend the domain to infinite space, while doubling the current strength.

Reaction 1 conserves two quantities, the total Ca^{2+} and total buffer concentrations; the corresponding two linear combinations of Eqs. 2 that cancel the reaction terms yield the two conservation laws (17, 18, 21, 29, 33, 34):

$$\begin{cases} \text{Ca}^{2+} \text{ conservation:} & \frac{\partial}{\partial t} (C + B^*) = \nabla^2 (D_C C + D_B^* B^*), \\ \text{Buffer conservation:} & \frac{\partial}{\partial t} (B + B^*) = \nabla^2 (D_B B + D_B^* B^*). \end{cases} \quad (3)$$

We will adopt the commonly used simplifying assumption that buffer diffusivity is not affected by the binding of a Ca^{2+} ion, $D_B = D_B^*$ (18). Under this assumption, buffer conservation reduces to $B + B^* = \text{const} = B_T$ (total buffer concentration B_T is constant in time and space). At equilibrium, Ca^{2+} conservation condition becomes (17, 18, 21, 29, 33, 34):

$$\nabla^2 (D_C C + D_B B^*) = 0. \quad (4)$$

For a collection of channels (point sources) on an infinite membrane with zero Ca^{2+} concentration at infinity, this Laplace's equation has a simple exact solution in terms of the free-space Green's function (21):

$$D_C C + D_B (B_T - B) = \frac{1}{2\pi z F} \sum_{k=1}^N \frac{I_{\text{Ca},k}}{|r - r_k|}. \quad (5)$$

Here the summation extends over individual open Ca^{2+} channels with current amplitudes $I_{\text{Ca},k}$, F is the Faraday constant, and $z=2$ is the valence of the Ca^{2+} ion. We can use the above two conservation laws to eliminate all but one equation in Eq. 2. Choosing to retain the unbound buffer concentration as the remaining variable, we obtain:

$$D_B \nabla^2 B = k^+ BC - k^- (B_T - B). \quad (6)$$

where Ca^{2+} concentration $[\text{Ca}^{2+}]=C$ can be eliminated using Eq. 5. Equations 5 and 6 completely describe the problem analyzed in this work. We will further restrict our analysis to the special case of a single channel at the origin, leading to a spherically symmetric solution. As noted above, we assume zero background Ca^{2+} concentration for the sake of simplicity, but the latter condition can be readily relaxed, as shown in the Appendix.

II.1 Non-dimensionalization

We non-dimensionalize Eqs. 5-6 following Smith et al. (18), normalizing Ca^{2+} and buffer concentrations by the buffer affinity and its total concentration, respectively: $c = C/K$, $b = B/B_T$, $b^* = B^*/B_T$, and introducing the dimensionless distance variable $\rho \equiv r(4\pi FK D_C)/I_{Ca}$, where I_{Ca} is the Ca^{2+} current and $K = k^-/k^+$ is the buffer affinity (dissociation constant). This normalizes the source strength to unity: $c(\rho) \approx 1/\rho$ as $\rho \rightarrow 0$. The dimensionless buffer conservation condition simplifies to $b + b^* = 1$. For the case of a single channel examined here, we obtain:

$$\begin{cases} \text{Unbound buffer:} & \lambda \nabla_{\rho}^2 b = c b + b - 1, \\ \text{Ca}^{2+} \text{ conservation:} & c = \nu(b-1) + 1/\rho, \\ \text{Boundary conditions:} & \lim_{\rho \rightarrow 0}(\rho^2 b_{\rho}) = 0, \quad \lim_{\rho \rightarrow 0}(\rho^2 c_{\rho}) = -1, \quad \lim_{\rho \rightarrow +\infty} b = 1, \quad \lim_{\rho \rightarrow +\infty} c = 0. \end{cases} \quad (7)$$

where ∇_{ρ}^2 is the spherically symmetric Laplacian operator, and the two remaining dimensionless parameters depend on the buffering properties, reactant diffusivities and the Ca^{2+} current amplitude (18):

$$\lambda = \left(\frac{4\pi FK D_C}{I_{Ca}} \right)^2 \frac{D_B}{k^-}, \quad \nu = \frac{B_T D_B}{K D_C}. \quad (8)$$

Here λ is the dimensionless buffer diffusion coefficient (denoted ε_b in (18)); it quantifies the ratio between the rate of Ca^{2+} diffusion on the one hand, and the rate of Ca^{2+} binding and Ca^{2+} influx on the other hand. Therefore, parameter regime $\lambda \ll 1$ corresponds to the Rapid Buffering approximation (RBA). Because λ depends on the Ca^{2+} current amplitude, the applicability of RBA and other asymptotic regimes may change with changing Ca^{2+} current, as reviewed below and discussed in (18).

The second parameter ν quantifies the overall buffering effectiveness, and equals the product of the resting buffering capacity, $\kappa = B_T/K$, and the relative buffer mobility, D_B/D_C . Some expressions will have a simpler form in terms of parameter $q = 1/(1+\nu)$, or in terms of the reciprocal denoted $\mu = 1/\nu$, as in (18). As the Ca^{2+} conservation condition in Eq. 7 shows, sufficiently close to the channel Ca^{2+} concentration is little perturbed from the free diffusion solution, $c = 1/\rho$, unless ν is sufficiently large ($\nu \gg 1$, $\mu \ll 1$; see Figs. 1-2). Example values of these parameters are given in Table 1 (cf. table 4.2 in (18)), for two widely expressed endogenous buffers and two exogenous buffers, and for several combinations of I_{Ca} values and total buffer concentration.

Combining the free buffer equation with Ca^{2+} conservation in Eq. 7 allows to eliminate the equation for free Ca^{2+} and yields a single ordinary differential equation on a semi-infinite domain $\rho > 0$ for the free buffer concentration, $b(\rho)$:

$$\lambda \nabla_{\rho}^2 b = (b-1)(\nu b + 1) + b/\rho. \quad (9)$$

where $\nabla_{\rho}^2 b$ is the spherical Laplacian. The boundary conditions are:

- $\lim_{\rho \rightarrow 0}(\rho^2 b_{\rho}) = 0$: no buffer flux at Ca^{2+} channel mouth

- $\lim_{\rho \rightarrow \infty} b(\rho) = 1$: buffer is free far from the channel ($B \rightarrow B_T$, so $b = B / B_T \rightarrow 1$)

This is a challenging equation as it represents a non-linear and singular boundary value problem. The concentration of buffer at the channel location, $b_0 = b(\rho=0)$, is not known *a priori*, which is crucial for the existence of a unique solution for any pair of parameter values λ and μ .

	$I_{Ca} = 0.1 \text{ pA}$		$I_{Ca} = 0.5 \text{ pA}$		$I_{Ca} = 2 \text{ pA}$	
	$B_T = 100 \mu\text{M}$	$B_T = 1 \text{ mM}$	$B_T = 100 \mu\text{M}$	$B_T = 1 \text{ mM}$	$B_T = 100 \mu\text{M}$	$B_T = 1 \text{ mM}$
BAPTA	$\lambda=0.28$ $\mu=0.0039$	$\lambda=0.28$ $\mu=0.00039$	$\lambda=0.011$ $\mu=0.0039$	$\lambda=0.011$ $\mu=0.00039$	$\lambda=0.00047$ $\mu=0.0039$	$\lambda=0.00047$ $\mu=0.00039$
EGTA	$\lambda=461$ $\mu=0.004$	$\lambda=461$ $\mu=0.0004$	$\lambda=18.4$ $\mu=0.004$	$\lambda=18.4$ $\mu=0.0004$	$\lambda=1.15$ $\mu=0.004$	$\lambda=1.15$ $\mu=0.0004$
Parvalbumin	$\lambda=0.851$ $\mu=0.0026$	$\lambda=0.851$ $\mu=0.00026$	$\lambda=0.034$ $\mu=0.0026$	$\lambda=0.034$ $\mu=0.00036$	$\lambda=0.0021$ $\mu=0.0026$	$\lambda=0.0021$ $\mu=0.00036$
ATP	$\lambda=1060$ $\mu=2.62$	$\lambda=1060$ $\mu=0.262$	$\lambda=42.5$ $\mu=2.62$	$\lambda=42.5$ $\mu=0.262$	$\lambda=2.66$ $\mu=2.62$	$\lambda=2.66$ $\mu=0.262$

Table 1. Values of dimensionless parameters λ and $\mu=1/\nu$ (Eq. 8) for several endogenous and exogenous Ca^{2+} buffers: BAPTA: $K_D=0.176 \mu\text{M}$, $k^- = 0.08 \text{ ms}^{-1}$, $D_B=0.1 \mu\text{m}^2/\text{ms}$ (35); EGTA: $K_D=0.18 \mu\text{M}$, $k^- = 0.5 \text{ s}^{-1}$, $D_B=0.1 \mu\text{m}^2/\text{ms}$ (35); parvalbumin: $K_D=0.0514 \mu\text{M}$, $k^- = 0.95 \text{ s}^{-1}$, $D_B=0.043 \mu\text{m}^2/\text{ms}$ (36-38); ATP: $K_D=200 \mu\text{M}$, $k^- = 45 \text{ ms}^{-1}$, $D_B=0.168 \mu\text{m}^2/\text{ms}$ (39). Ca^{2+} diffusivity was set to $D_C=0.220 \mu\text{m}^2/\text{ms}$ (40). For a buffer with multiple identical Ca^{2+} binding sites, B_T is defined as the concentration of binding sites.

II.2 Previously developed approximations

The study of Smith et al. (18) provided a rigorous analysis and review of distinct asymptotic approximations for stationary Ca^{2+} nanodomains and showed that, with the exception of the Linear approximation (LIN), these methods can be understood as asymptotic expansions of the solution with respect to two nondimensional parameters $\mu=1/\nu$ and λ given by Eqs. 8. These approximations are summarized below, focusing for the sake of simplicity on the special case of zero background Ca^{2+} concentration ($c_x=0$, $b_x=1$):

- Excess Buffer approximation (EBA) (15, 18, 27) is an expansion in μ around free-buffer solution $b=1$ for $\lambda\mu = O(1)$ (the $O(\mu)$ term in $c(\rho)$ is derived in (18)):

$$b(\rho) = 1 + \mu \left[\exp(-\rho/\sqrt{\mu\lambda}) - 1 \right] / \rho + O(\mu^2); \quad c(\rho) = \exp(-\rho/\sqrt{\mu\lambda}) / \rho + O(\mu). \quad (10)$$

- Linear approximation (LIN) (15, 18, 23, 30, 31) is a linearization around constant equilibrium baseline $b=1$, $c=0$; expressed in terms of parameter $q = 1/(1 + \nu) = \mu/(1 + \mu)$, it yields

$$b(\rho) = 1 + q \left[\exp(-\rho/\sqrt{q\lambda}) - 1 \right] / \rho; \quad c(\rho) = \left[q + (1 - q) \exp(-\rho/\sqrt{q\lambda}) \right] / \rho. \quad (11)$$

- Rapid Buffering approximation (RBA) (15, 17, 18, 21, 27-30, 41) is a singular perturbation expansion in parameter λ around reaction equilibrium solution, with $\mu=O(1)$. Following (18), we define the corresponding expansions up to orders $O(1)$ and $O(\lambda)$ as 1st- and 2nd-order RBA, respectively:

$$b(\rho) = \frac{\mu}{2} \left[-\frac{1}{\rho} - \frac{\mu-1}{\mu} + \left(\left(\frac{1}{\rho} + \frac{\mu-1}{\mu} \right)^2 + \frac{4}{\mu} \right)^{1/2} \right] + 2\lambda \left[\left(1 + \rho \frac{\mu-1}{\mu} \right)^2 + \frac{4\rho^2}{\mu} \right]^{-2} + O(\lambda^2). \quad (12)$$

- Nearly Immobile Buffer approximation (IBA), derived in (18), corresponds to $\lambda \ll 1$, $\lambda\mu = O(1)$ ($\nu \ll 1$):

$$b(\rho) = \frac{\rho}{1+\rho} + \frac{2\lambda}{(1+\rho)^4} + \frac{\nu\rho^2}{(1+\rho)^3} + O(\lambda^2); \quad c(\rho) = \frac{1}{\rho} - \frac{\nu}{(1+\rho)} + O(\lambda^2). \quad (13)$$

As noted above, EBA and LIN provide a convenient approximation for the space constant of exponential nanodomain Ca^{2+} decay as a function of distance from channel location. In contrast to EBA and IBA, RBA and the LIN satisfy Ca^{2+} conservation, and therefore Ca^{2+} and buffer concentrations are related to each other by the condition $c = 1/\rho + \nu(b-1)$ (Eq.7). This feature is also shared by the approximation proposed in this study. As discussed in (18), LIN reduces to EBA when $\mu \ll 1$, and the regions of applicability of EBA and LIN approximations substantially overlap. Therefore, we will only use LIN and RBA to analyze the relative accuracy of the newly presented approximation method (see Figs. 2-6), since these two approximations methods are accurate over a wider range of buffering conditions compared to EBA and IBA, as shown in (18).

We note two critical simplifying assumptions inherent in the above-mentioned and the newly presented approximation methods. First, these approximations for Ca^{2+} concentration are only to be used above the spatial scale of the channel pore radius, since the point-channel idealization and the infinite concentration at the channel location in Eqs. 5, 10-13 are clearly unphysical: Ca^{2+} concentration reaches a finite value at the channel pore. In fact, the dependence of Ca^{2+} current on the finite Ca^{2+} concentration gradient across the pore determines the unitary steady-state channel current amplitude (42, 43). Second, the effect of Ca^{2+} pump is neglected, which will affect the accuracy of the approximation far from the channel. The contribution of linearized endoplasmic reticulum Ca^{2+} pumps to steady-state Ca^{2+} concentration approximation has been explored in (43).

III. RESULTS

As was emphasized by Smith et al. (18) and is demonstrated in Table 1, the applicability conditions of the previously developed approximations depend not only on intrinsic, fixed properties of Ca^{2+} buffers, but also depend on the magnitude of the Ca^{2+} current through the non-dimensional parameter λ . Thus, the accuracy of a particular approximation method will vary with the magnitude of the Ca^{2+} current, as well as the buffering parameters such as total buffer concentration. The primary motivation for the work presented here is to seek alternative approximations with more uniform accuracy with respect to the model parameters λ and μ , seeking a method that could potentially be extended to cooperative buffers with two Ca^{2+} -binding sites. In developing such a method, we will use two distinct series representations of the solution to Eq. 9, and will take advantage of its monotonicity in ρ and its boundedness (see Fig. 1).

III.1 Short-range Taylor series

Eq. 9 has only a regular singularity at $\rho=0$, and therefore it *does* have a solution analytic at $\rho=0$, representing the physical nanodomain solution that we seek. Interestingly, buffer concentration does not vanish at $\rho=0$ (see Fig. 1A1,B1,C1) despite unbounded Ca^{2+} concentration at the channel mouth: $b(0)=b_0 \neq 0$ (EBA and RBA approximate the value of b_0 as $1 - (\mu/\lambda)^{1/2}$ and 2λ , respectively). Apart from solving Eq. 9 numerically, one can examine the solution's Taylor series in ρ :

$$b(\rho) = \sum_{n=0}^{\infty} b_n \rho^n = b_0 + \frac{b_0 \rho}{2\lambda} + \frac{(b_0 - 1)(1 + \nu b_0) + b_0 / (2\lambda)}{6\lambda} \rho^2 + O(\rho^3). \quad (14)$$

This relationship between coefficients in the ρ -series will be used by the method developed below. Numerical exploration showed that this Taylor series has a finite radius of convergence that depends both on μ and λ , and for a wide range of these buffering parameters the convergence radius extends to around $\rho \sim 1$. The 3rd order Taylor polynomials are shown as blue curves in Fig. 1, for three distinct sets of parameter values. As mentioned above, the boundary value of $b(0) = b_0$ is unknown *a priori* and has to be determined by the approximate solution.

III.2 Long-range asymptotic series

We will attempt to match the short-range series given by Eq. 14 with the large- ρ (long-range) behavior, analyzed by making a coordinate mapping $x \equiv 1/\rho$ in Eq. 9, which transforms this equation to

$$\lambda x^4 b_{xx} = (b-1)(\nu b+1) + bx, \quad b(x=0) = 1. \quad (15)$$

Although the Laplacian formally simplifies in the new variable x , this inversion map reveals an *essential* singularity at $x=0$ (the power of x multiplying the second derivative is higher than 2). Straightforward coefficient matching allows to find the following *unique* series solution near $x=0$ satisfying $b(x=0)=1$ (buffer is free infinitely far from channel; see Appendix for non-zero $[Ca^{2+}]$ at $x=0$):

$$b(x) = 1 + \sum_{n=1}^{\infty} \beta_n x^n = 1 - qx + q^3 x^2 - q^4 (2q-1) x^3 + q^4 [2\lambda + q(1+5q(q-1))] x^4 + O(x^4). \quad (16)$$

Here we used parameter $q = 1/(1+\nu) = \mu/(1+\mu)$ to simplify the coefficients. Because Eq. 15 has an *essential* singularity at $x=0$, the obtained series is only an asymptotic series that the physical solution we seek approaches as $x=1/\rho \rightarrow 0$. Therefore, it does *not* converge for any finite value of $x=1/\rho$, but provides a good approximation to the true solution for any finite order, as shown in Fig. 1 (*red curves*). It is interesting to observe that for $\mu=1$ ($q=1/2$) and $\lambda=1/16$ this system has an *exact* (finite) quadratic asymptotic $b(x) = 1 - x/2 + x^2/8$. There is an inherent connection between this long-range expansion and other approximations: terms in Eq. 16 up to $O(x^3)$ agree with IBA (Eq.13), provided $\nu \ll 1$, while terms up to $O(x^5)$ agree with RBA (Eq. 12). This illustrates that reaction is approximately at equilibrium far from channel: note that reaction terms sum to zero at least up to order x^3 .

III.3 Method 1: continuous match between the long- and short-range series

While the ranges of applicability of the Taylor series in ρ and the asymptotic series in x are complementary to each other, these series representations may be close to each other at intermediate distances $\rho \sim 1$, $x \sim 1$. This suggests a simple way of approximating the full solution demonstrated in Fig. 1, whereby one seeks a continuous match of these two series representations at some intermediate value ρ^* (denoted by a vertical dotted line). This involves numerical minimization of the difference between the values of two truncated series and their first derivatives at some intermediate coordinate ρ^* , with respect to parameters ρ^* and b_0 . This optimization procedure therefore provides approximate solution for the boundary value b_0 . In Figure 1, the stitching is achieved numerically (using the *fminsearch* routine in MATLAB, Mathworks, Inc.) for $m=3$ and $n=2$, for three distinct values of parameters, and the resulting piece-wise polynomial function (*red and blue curves*) gives a good approximation of the exact solution estimated numerically (*black dashed curves*). Although the existence of a continuous optimizer is not in general guaranteed (note the discontinuity in Fig.

1B2), this simple method provides a good estimate for the solution for a wide range of model parameters λ and μ .

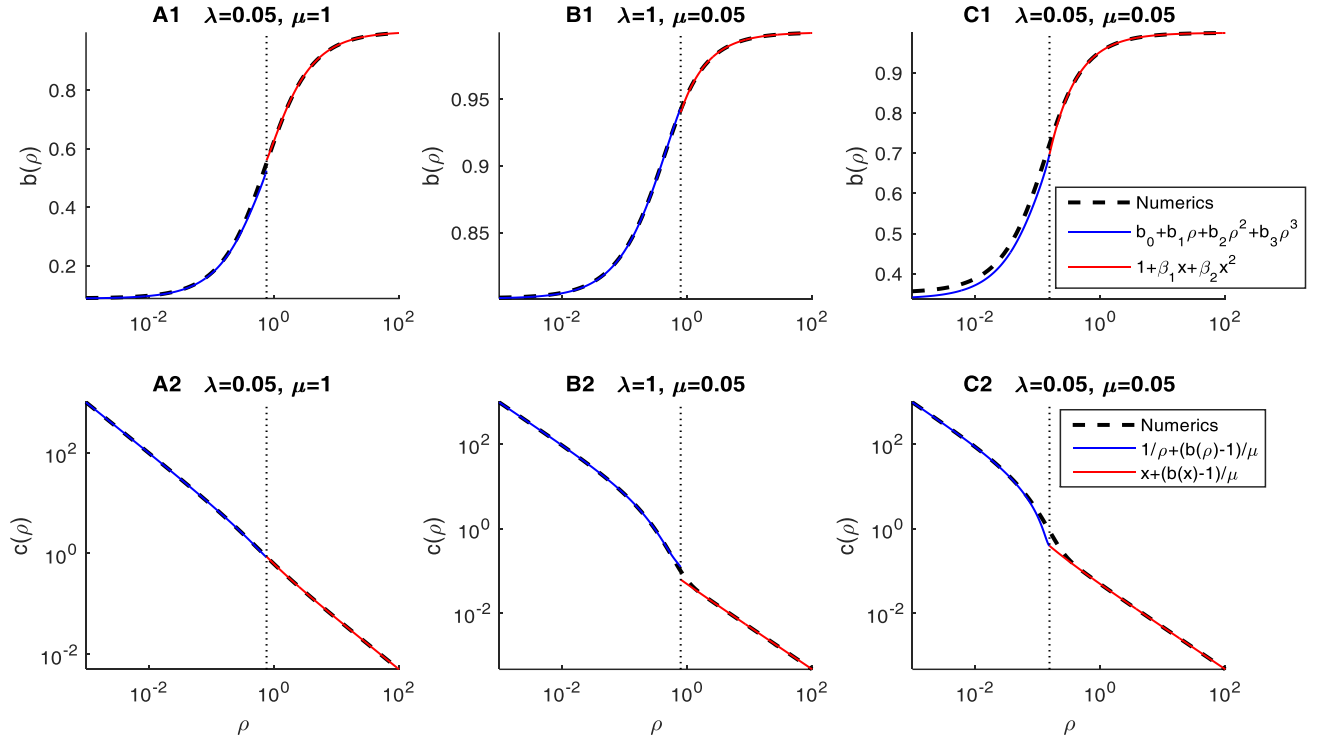


Figure 1. Matching short-range Taylor series (blue; 3rd order in ρ) and long-range asymptotic series (red; 2nd order in $x=1/\rho$) yields an accurate approximation of the numerically computed single-channel nanodomain profile (black dashed curve). A1, B1, C1: the dimensionless buffer concentration, $b(\rho)$, as a function of distance from the Ca^{2+} channel, for the three indicated choices of model parameters λ and μ . A2, B2, C2: corresponding dimensionless Ca^{2+} concentration, $c = 1/\rho + (b-1)/\mu$, on a logarithmic concentration scale. The value of $b(\rho=0)$ and the “stitching” argument value ρ^* (vertical dotted lines) are chosen to minimize the difference between the two polynomials and their derivatives at the stitching point, ρ^* . Parameter values in (A1, B1) correspond to the RBA regime $\lambda \ll 1$, $\mu = O(1)$; (A2, B2) correspond to the LIN regime, while neither RBA nor LIN are accurate for $\lambda = \mu = 0.05$ (A3, B3; cf. Fig. 2). Note that Ca^{2+} concentration is close to the free (unbuffered) nanodomain profile $c(\rho) = 1/\rho$, unless $\mu \ll 1$, as in B2, B3. Continuous match is not achieved for parameter values in (B1, B2).

When solving for the optimal match analytically rather than numerically, polynomial truncation of the ρ and x series up to order m and n , respectively, leads to a polynomial equation of order $m+n$. Therefore, the stitching continuity conditions cannot be solved in closed form for any order higher than $m+n=4$, and even in that case the resulting expressions could be prohibitively complex. Although a very simple closed-form solution is available for first-order linear case ($m=n=1$), we find the corresponding result to be rather inaccurate.

As demonstrated in Figure 1 and noted earlier, the relative deviation of the Ca^{2+} concentration from the free diffusion case ($c(\rho)=1/\rho$) is small sufficiently close to the channel unless buffering is strong, i.e. unless $\mu \ll 1$ ($\nu \gg 1$).

III.4 Method 2: dual-Padé Approximation

As mentioned above, one drawback of the piece-wise match method is that the existence and uniqueness of a smooth match is not guaranteed, and that it is inaccurate at the lowest order for which analytic continuity

conditions can be obtained. Here we present an alternative approach, which we find to be more accurate for the same truncation order, and which yields a unique smooth approximation. This approach involves a rational function *Ansatz* to simultaneously match leading terms of the low- ρ (short-range) series described by Eq. 14 and the low- x (long-range, high- ρ) series given by Eq. 16:

$$b\left(x = \frac{1}{\rho}\right) = \frac{1 + A_1 x + A_2 x^2 + \dots + A_n x^n}{1 + B_1 x + B_2 x^2 + \dots + B_n x^n} = \frac{\rho^n + A_1 \rho^{n-1} + \dots + A_n}{\rho^n + B_1 \rho^{n-1} + \dots + B_n}. \quad (17)$$

This can be viewed as a “dual” Padé approximation that simultaneously matches two distinct series representations up to order n , in contrast to the standard Padé method, which matches a single series up to order $2n$. Imposing additional constraints $B_k > A_k > 0$ and $B_{k+1} / A_{k+1} > B_k / A_k > 1$ enables us to satisfy two important physical constraints: the free buffer concentration $b(\rho)$ is bounded and monotonically increasing from $b_0 \geq 0$ at the channel mouth to $b(\rho \rightarrow \infty) = 1$ infinitely far from the channel.

It is instructive to consider carefully the lowest-order dual-Padé approximation, namely $n=1$, corresponding to the primitive bilinear function approximation:

$$b\left(x = \frac{1}{\rho}\right) = \frac{1 + A_1 x}{1 + B_1 x} = \frac{\rho + A_1}{\rho + B_1}. \quad (18)$$

Expanding this rational function in a Taylor series around $\rho=0$ yields

$$b(\rho) = \frac{A_1}{B_1} + \frac{B_1 - A_1}{B_1^2} \rho + O(\rho^2). \quad (19)$$

On the other hand, expanding the same function in a series around $x=0$ yields

$$b(x) = 1 + (A_1 - B_1)x + O(x^2). \quad (20)$$

Comparing these expansions with Eqs. 14 and 16 yields 3 constraints for the 3 unknowns, A_1 , B_1 and b_0 :

$$b_0 = \frac{A_1}{B_1}, \quad b_1 = \frac{b_0}{2\lambda} = \frac{B_1 - A_1}{B_1^2}, \quad B_1 - A_1 = \frac{1}{1+\nu}. \quad (21)$$

This nonlinear system has a unique solution satisfying monotonicity and boundedness conditions:

$$A_1 = \frac{-1 + [1 + 8\lambda(1+\nu)]^{1/2}}{2(1+\nu)}, \quad B_1 = \frac{1 + [1 + 8\lambda(1+\nu)]^{1/2}}{2(1+\nu)}. \quad (22)$$

Figure 2 shows surprisingly decent performance of the primitive rational approximation given by Eqs. 18, 22 (*solid red curves*), as compared with the more sophisticated Rapid Buffering approximation (RBA, *blue curves*) and the Linear approximation (LIN, *green curves*). Note also that the approximate solution for Ca^{2+} (Fig. 2A2, B2, C2) is harder to distinguish by eye from the exact solution, due to the dominance of the $1/\rho$ free diffusion term near the channel mouth.

In dimensional form, the Ca^{2+} and buffer concentrations corresponding to the lowest-order, bilinear approximation are given by

$$[\text{Buffer}] = B_{\text{Total}} \frac{r + \hat{A}_1}{r + \hat{B}_1}, \quad [\text{Ca}^{2+}] = \frac{I_{\text{Ca}}}{4\pi D_C F r} + \frac{B_T D_B}{D_{\text{Ca}}} \frac{\hat{A}_1 - \hat{B}_1}{r + \hat{B}_1}. \quad (23)$$

where $\hat{A}_1 = A_1 I_{\text{Ca}} / (4\pi F K D_C)$, $\hat{B}_1 = B_1 I_{\text{Ca}} / (4\pi F K D_C)$ have dimensions of length, and F is the Faraday constant.

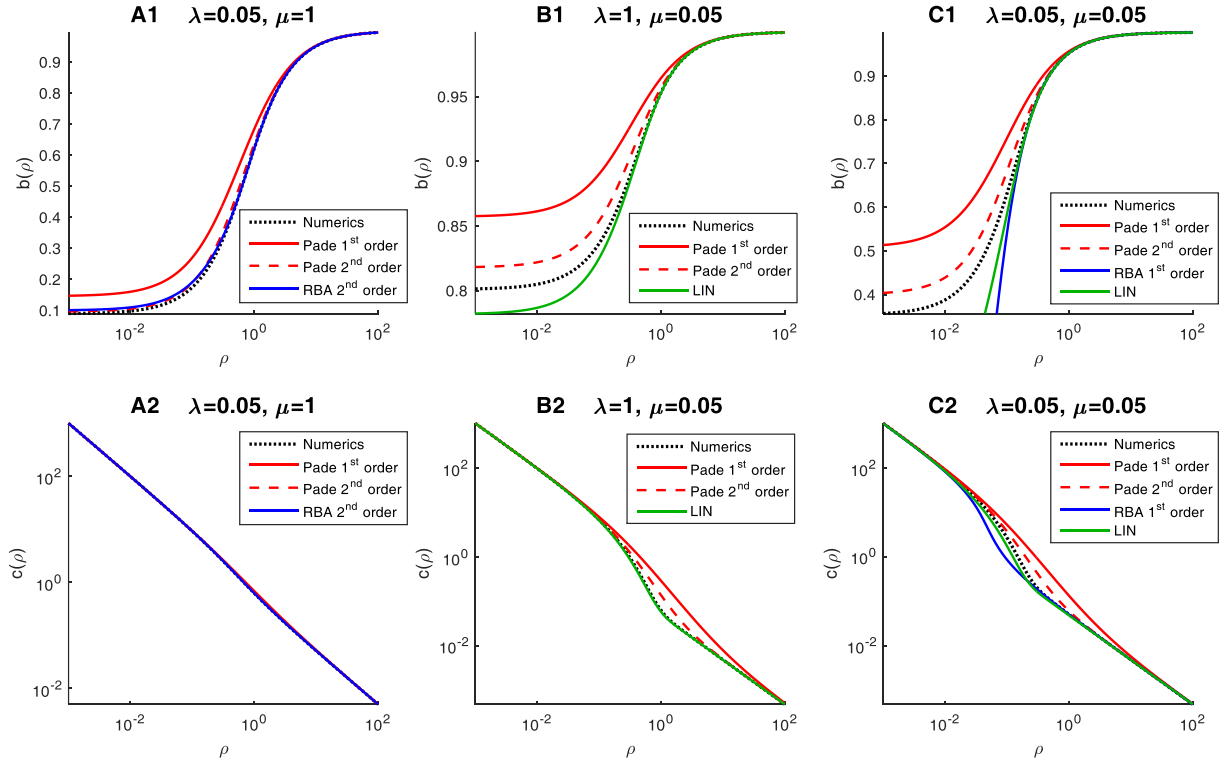


Figure 2. Comparison of the rational approximation (Padé, *red curves*) with the Linear (LIN, *green curves*) and Rapid Buffer (RBA, *blue curves*) approximations for the equilibrium single-channel domain. *A1, B1, C1*: free dimensionless buffer concentration as a function of distance from the Ca^{2+} channel, for 3 distinct choices of model parameters λ and μ . *A2, B2, C2*: free dimensionless Ca^{2+} concentration as a function of distance from the channel, on logarithmic scale. Dashed black curves show the accurate numerical solution. Note that the lowest-order, bilinear approximation (*red solid curves*, Eq. 22) is less accurate than RBA (*blue curves* in *A1, A2*) and comparable to LIN (*green curves* in *B1, B2*) in their respective parameter regimes, but its approximation of buffer concentration is superior for $\mu=\lambda=0.05$ (*C1, C2*), where neither RBA nor LIN is applicable. Finally, 2nd-order rational approximation (*red dashed curves*, Eq. 17) is as accurate as RBA (*A1, A2*) and LIN (*B1, B2*), and yields a far more accurate buffer estimate for $\mu=\lambda=1$ (*C1*). Since 2nd order RBA is inaccurate for $\mu=\lambda=0.05$, 1st order RBA is shown in (*C1, C2*). Note the change in scale in (*B1*): the relative error of 1st order Padé approximation is within 6% of true solution.

As results in Figure 2 demonstrate, the ratio of quadratic functions (*dashed red curves*) is even more accurate, and is superior to RBA and LIN in approximating buffer concentration for all three chosen pairs of parameter values. However, it should be noted that RBA has one important advantage in that it can be generalized to the case of multiple channels (21). Therefore RBA is a particularly powerful method whenever its applicability conditions $\lambda \ll 1$, $\lambda\mu = O(1)$ are satisfied.

Another drawback of the Padé approach is the complexity of algebra beyond the leading order. Let's consider for example the 2nd order approximation. As in the case of bilinear approximation (Eqs. 17-20), we start with the dual expansions of the rational function:

$$b(\rho) = \frac{\rho^2 + A_1\rho + A_2}{\rho^2 + B_1\rho + B_2} = \frac{A_2}{B_2} + \frac{A_1B_2 - A_2B_1}{B_2^2}\rho + \frac{B_2(B_2 - A_2) - B_1(A_1B_2 - B_1A_2)}{B_2^3}\rho^2 + O(\rho^3), \quad (24)$$

$$b(x) = \frac{1 + A_1x + A_2x^2}{1 + B_1x + B_2x^2} = 1 + (A_1 - B_1)x + [B_1(B_1 - A_1) + A_2 - B_2]x^2 + O(x^3). \quad (25)$$

Matching the coefficients of these two series expansions with Eqs. 14,16 yields the following 5 constraints for the 5 unknowns, $A_{1,2}$, $B_{1,2}$ and b_o (cf. Eq. 21, and recall that $q = 1 / (1 + \nu) = \mu / (1 + \mu)$):

$$\left\{ \begin{array}{l} b_o = \frac{A_2}{B_2}, \quad \frac{b_o}{2\lambda} = \frac{A_1 B_2 - A_2 B_1}{B_2^2}, \quad \frac{(b_o - 1)(1 + \nu b_o) + b_o / (2\lambda)}{6\lambda} = \frac{B_2(B_2 - A_2) - B_1(A_1 B_2 - A_2 B_1)}{B_2^3}, \\ B_1 - A_1 = q, \quad B_2 - A_2 = q(B_1 - q^2). \end{array} \right\} \quad (26)$$

After extensive algebraic simplification, one obtains two coupled quadratic equations for B_1 and B_2 (coefficients A_1 and A_2 are then found using the last two equations in Eq. 26):

$$\left\{ \begin{array}{l} 2\lambda B_1^2 + B_1 B_2 - B_2^2 / q - 2\lambda q^2 B_1 - (q^2 + 2\lambda) B_2 = 0, \\ (1 + q) B_1^2 - 2 B_1 B_2 / q + 2(3\lambda - q^3) B_1 + (1 - q) B_2 = q^2 (6\lambda + q^2 (1 - q)). \end{array} \right. \quad (27)$$

This system has a unique, closed-form solution satisfying given physical constraints. However, this solution is too lengthy to show in print. Padé approximations of third order and higher are given by even more complicated polynomial system, with no closed-form solution for general values of λ and $\nu = 1/\mu$. However, for any particular set of parameter values, the coefficients are readily calculated directly or by substituting parameter values into obtained analytic expressions. For instance, below is the dual-Padé representation for the case $\lambda = \mu = 1$ (see Fig. 7), obtained by rounding to 52 bits the closed-form solution obtained using MATLAB's symbolic toolbox (Mathworks, Inc.):

$$b(\rho) = \frac{2^{52} \rho^2 + 8494216396637444 \rho + 5511819248185369}{2^{52} \rho^2 + 10746016210322694 \rho + 10321877399925404}. \quad (28)$$

We emphasize that it matches *exactly* the long-range series up to 2nd order in x , and the relationship between coefficients in the quadratic Taylor polynomial in ρ . Given fixed values of parameters μ and λ , we were able to obtain unique solutions for coefficients of the dual-Padé approximation up to fifth order and higher; the corresponding MATLAB code is given in Supplementary Information. Figure 3 shows that Padé approximations of increasing order quickly converge to the exact solution.

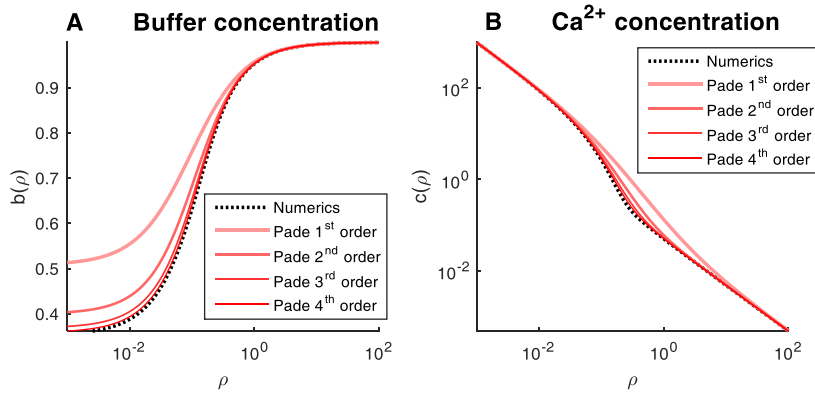


Figure 3. Convergence of Padé approximations of increasing order (*solid red-shade lines*) to the numerically computed solution (*dotted line*) for $\mu = \lambda = 0.05$ (cf. Fig. 2C1, 2C2). Note that the 4th order Padé approximation is visually indistinguishable from the exact solution on the given axis resolution scale.

As Figure 2 shows, both the previously developed approximations and the newly presented method have the lowest accuracy near the channel, and the greatest accuracy far from the channel, since the asymptotic

behavior for $x \rightarrow 0$ is determined by the Dirichlet boundary condition corresponding to the resting background Ca^{2+} concentration infinitely far from channel. However, when comparing free Ca^{2+} concentration the loss of accuracy close to the channel is compensated by the fact that the singular free diffusion term $1/\rho$ dominates $[\text{Ca}^{2+}]$ near the channel mouth (see Figs. 1A2, B2, C2).

Figures 4, 5 quantify the accuracy of estimating the free buffer and free Ca^{2+} concentrations, respectively, comparing the presented Padé method (Fig. 4C,4D,5C,5D) with RBA (Figs. 4A, 5A) and LIN (Figs. 4B, 5B), for a wide range of parameters λ and μ spanning 6 orders of magnitude. Following Smith et al. (cf. Fig. 9.2 in (18)), in Figure 4 we use an absolute deviation measure to quantify the accuracy in buffer concentration, while a logarithmic deviation measure is used to quantify the accuracy in Ca^{2+} concentration, in view of the unbounded $1/\rho$ behavior close to the source (channel):

$$\|b_{\text{approx}} - b_{\text{numer}}\| = \frac{1}{N} \sum_{n=1}^N |b_{\text{approx}}(\rho_n) - b_{\text{numer}}(\rho_n)|, \quad (29)$$

$$\|c_{\text{approx}} - c_{\text{numer}}\| = \frac{1}{N} \sum_{n=1}^N |\log c_{\text{approx}}(\rho_n) - \log c_{\text{numer}}(\rho_n)|. \quad (30)$$

The two deviations measures are computed on a set of $N=100$ points spanning 5 orders of magnitude of distance ρ , from 10^{-3} to 10^2 , on a logarithmic scale: $\rho_n = 10^{-3+5n/100}$ ($n=1, 2, \dots, N$). The gray shade in Figs. 4 and 5 indicates base-10 logarithm of these deviation measures, with unshaded region corresponding to the average deviation of 10^{-3} , which would be too small to resolve by naked eye. As can be inferred from Figs. 2A1,B1,C1, the error in estimating buffer concentration quantified by Eq. 29 is to large degree determined by the error in estimating the boundary value of buffer concentration at channel location (b_0). Figure 6 summarizes the data in Figs. 4-5, showing the regions in parameter space where each of the main approximations (RBA, LIN and 2nd order Padé) achieves superior accuracy relative to the other two.

Despite the fact that the newly presented method conserves Ca^{2+} concentration, and therefore buffer and Ca^{2+} concentrations can be readily derived from one another, the Padé approximation seems to provide much greater accuracy in estimating the free buffer rather than the free Ca^{2+} concentration (cf. Fig. 6A and Fig. 6B). In fact, Figs. 5 and 6B show that the 2nd order Padé approximation achieves superior accuracy in estimating Ca^{2+} concentration relative to RBA and LIN only in a narrow region of parameter space. It may appear counter-intuitive that the accuracy in Ca^{2+} estimation does not seem to match the accuracy in estimating free buffer concentration, despite the one-to-one relationship between the two. This apparent paradox is a result of the difference in the two deviation measures given by Eqs. 29-30. While the deviation between exact and approximate buffer concentration is the largest near the channel mouth for all methods studied, the relative or logarithmic Ca^{2+} concentration deviation measure is not sensitive to a finite error near the channel location, since it is dominated by the free diffusion term $1/\rho$ close to the channel: $c(\rho) = v(b(\rho) - 1) + 1/\rho$. Therefore, the relative error in Ca^{2+} concentration approximation is particularly sensitive to the accuracy of the method at intermediate values of distance, rather than its accuracy in the vicinity of the channel.

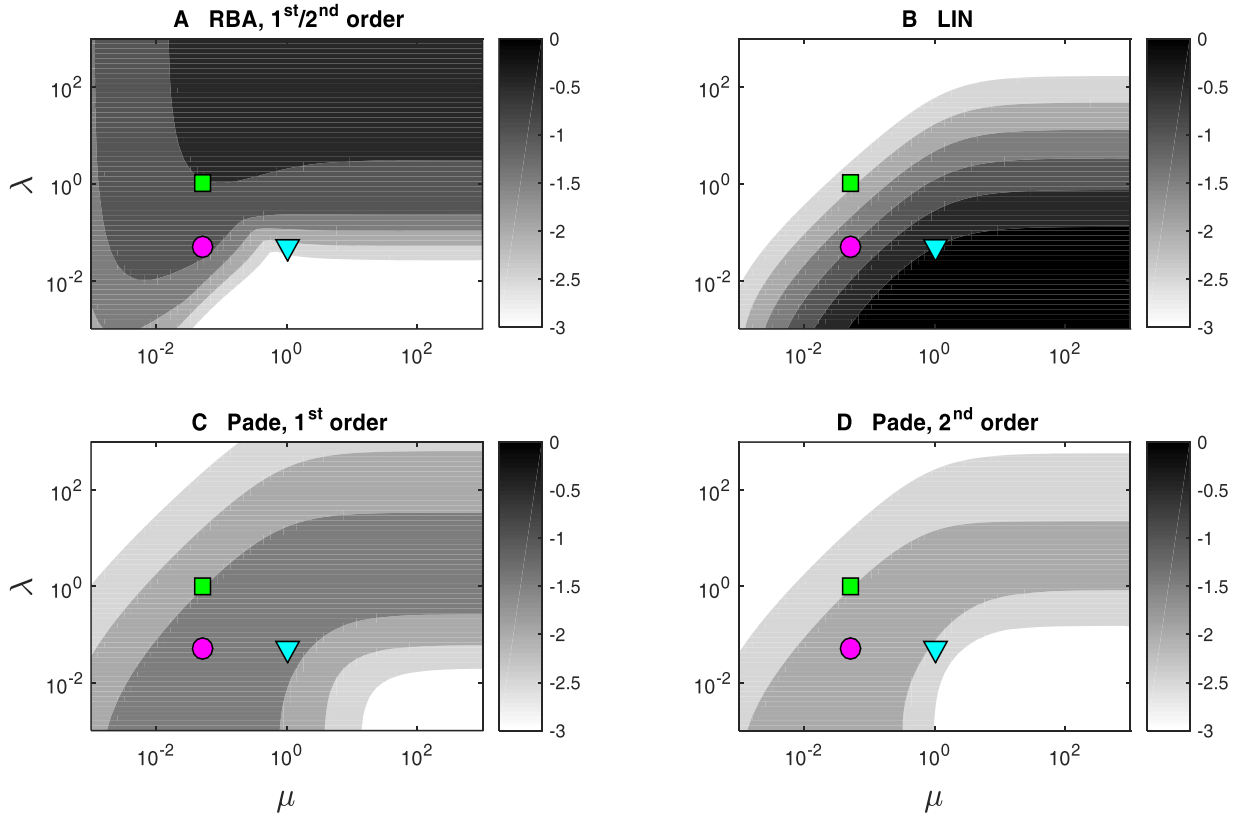


Figure 4. Accuracy of free buffer concentration estimation by the dual-Padé approximation (C, bilinear order; D, quadratic order), as compared to the RBA (A) and LIN (B) approximations. In (A), either 1st or 2nd order of RBA approximation is used, whichever is more accurate, for each pair of parameter values μ and λ . The six contour lines correspond to the average absolute deviation (see Eq. 29) of 10^{-3} (white), $10^{-2.5}$, 10^{-2} , $10^{-1.5}$, 10^{-1} , and $10^{-0.5}$ (black). Symbols mark the three sets of model parameters examined in Figs. 1-2: *triangle*: $\mu=1$, $\lambda=0.05$ (RBA regime); *square*: $\mu=0.05$, $\lambda=1$ (LIN regime); *circle*: $\mu=\lambda=0.05$ (neither RBA nor LIN is accurate). (neither RBA nor LIN is accurate).

IV. Discussion

As early modeling studies of cell Ca^{2+} diffusion and buffering demonstrated (11-14, 44), quasi-stationary Ca^{2+} concentration domains are established within a fraction of millisecond after the opening of a single channel, and collapse as rapidly after the channels close. This suggests that simple, closed-form approximations to the stationary single-channel nanodomains often provide sufficient accuracy in estimating Ca^{2+} and buffer concentration in the vicinity of a Ca^{2+} channel, allowing to avoid costly reaction-diffusion deterministic or stochastic simulations. Here we presented an initial attempt at extending previous work on such approximate solutions, introducing a qualitatively new type of approximation that takes advantage of two properties of the exact solution that previous approximations did not explicitly use: (i) the long-range asymptotic series representation of the solution in powers of reciprocal distance, and (ii) the monotonic, bounded character of the free buffer concentration. Even at lowest order, the resulting Padé approximation achieves a decent estimate for the free buffer and Ca^{2+} concentration near an open channel, for several orders of magnitude of dimensionless parameters λ and μ . Although the presented method is particularly accurate in estimating free buffer concentration, it can also provide accuracy improvement in estimating free Ca^{2+} as well, given sufficiently large values of μ (Fig. 4C,D; Fig. 5).

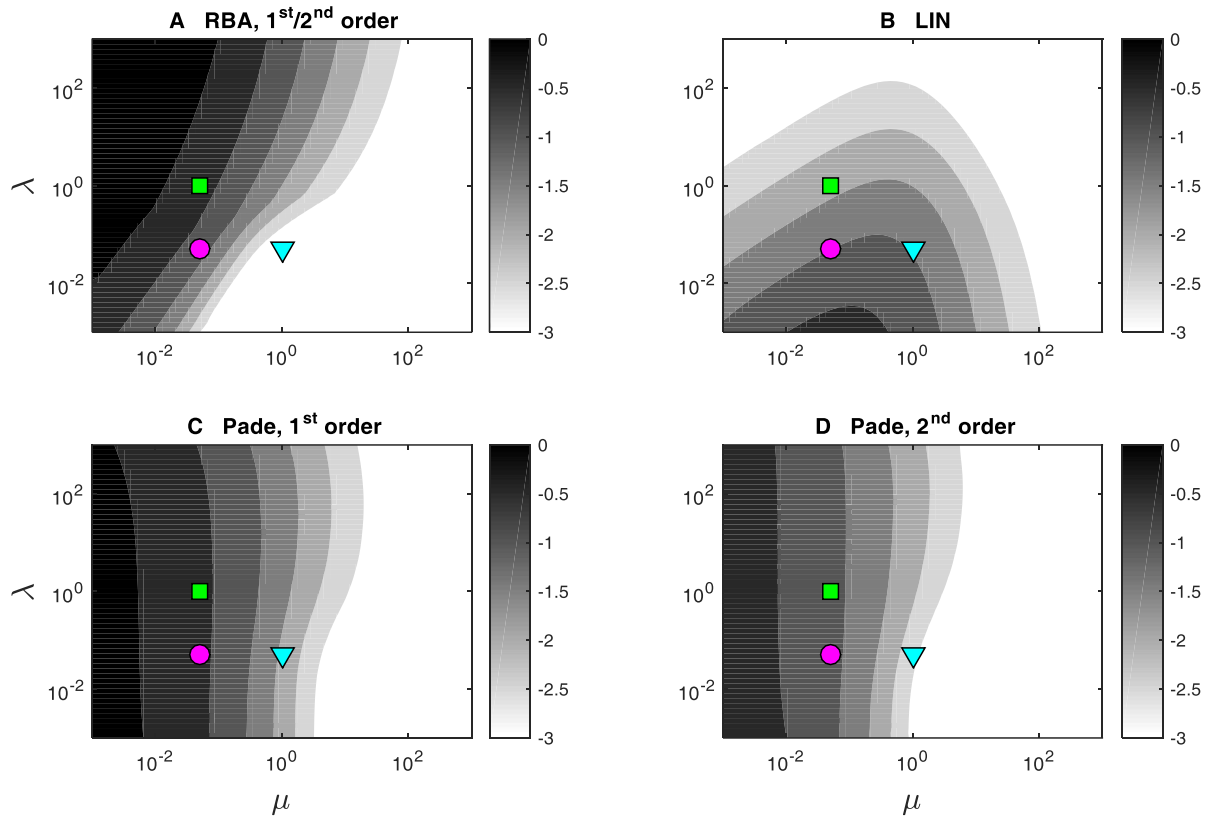


Figure 5. Accuracy in Ca^{2+} concentration estimation by the dual-Padé approximation (*C*, bilinear order; *D*, quadratic order), as compared to the RBA (*A*) and LIN (*B*) approximations. In (*A*), either 1st or 2nd order of RBA approximation is used, whichever is more accurate, for each pair of parameter values μ and λ . The six contour lines correspond to the average relative (logarithmic) deviation norm (see Eq. 30) of 10^{-3} (white), $10^{-2.5}$, 10^{-2} , $10^{-1.5}$, 10^{-1} , and $10^{-0.5}$ (black). Symbols mark the three sets of model parameters examined in Figs. 1-2: *triangle*: $\mu=1$, $\lambda=0.05$ (RBA regime); *square*: $\mu=0.05$, $\lambda=1$ (LIN regime); *circle*: $\mu=\lambda=0.05$ (neither RBA nor LIN is accurate).

The drawback of the newly presented method is that the expression for the coefficients of the rational function become very complex for any order higher than bilinear, requiring the use of a computer algebra system. However, we view the Padé approximation as only the first example of a new class of bounded, monotonic approximations that combine information about the short- and long-range behavior, and which can be improved by seeking a more accurate Ansatz. For example, one could attempt to match the singularities of the analytic extension of the true solution to the complex- ρ plane, starting with the behavior for negative values of ρ shown in Fig. 7 for the particular case $\lambda=\mu=1$ (see Eq. 28). The presented rational approximation does not match the behavior of the solution as $\rho \rightarrow -\infty$. As Figure 7 shows, $b \rightarrow -\mu$ in this limit, with no poles on the real $\rho < 0$ axis, while the Padé approximations always approaches unity as $\rho \rightarrow -\infty$. Further, some Padé approximants may have poles on the negative real axis: for instance, the bilinear approximation given by Eq. 18 has an obvious singularity at $\rho = -B_1$, contrary to the exact solution shown in Fig. 7. This suggest a possibility for significant improvement by seeking an Ansatz which matches the behavior of the analytic extension of the true solution seen in Fig. 7. The singularities of the true solution in the complex- ρ plane could also be examined.

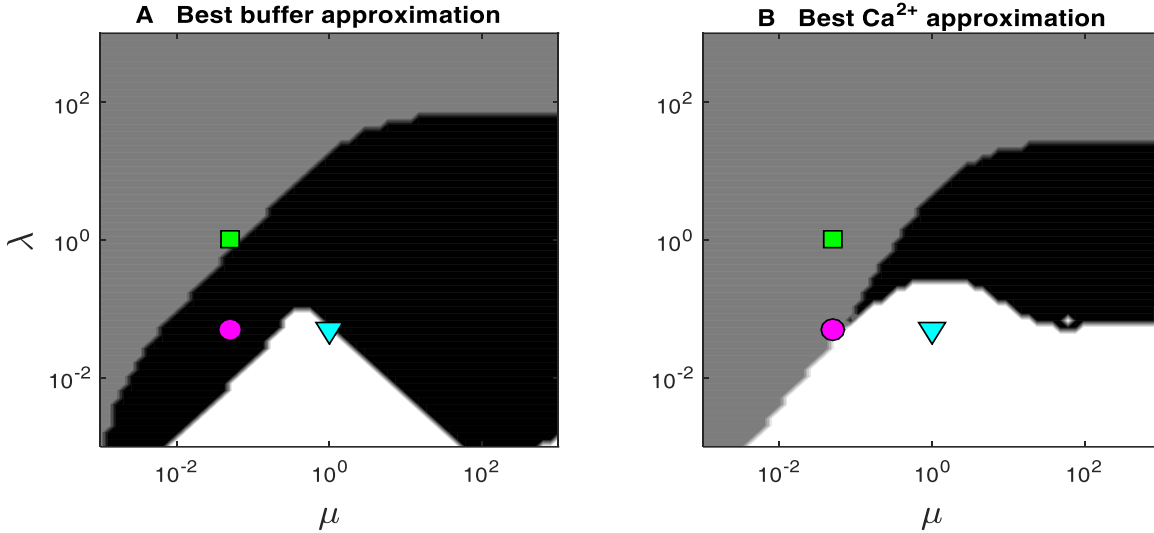


Figure 6. Comparison of parameter regions of smallest error in estimating (A) buffer and (B) Ca^{2+} concentration. *White*: region of best performance of 1st or 2nd order RBA; *gray*: region of best performance of LIN; *black*: region of best performance of the 2nd order Padé approximation. These plots summarize data shown in Figs. 4, 5. Symbols mark the three sets of model parameters examined in Figs. 1-2: *triangle*: $\mu=1$, $\lambda=0.05$ (RBA regime); *square*: $\mu=0.05$, $\lambda=1$ (LIN regime); *circle*: $\mu=\lambda=0.05$ (Padé approximation regime).

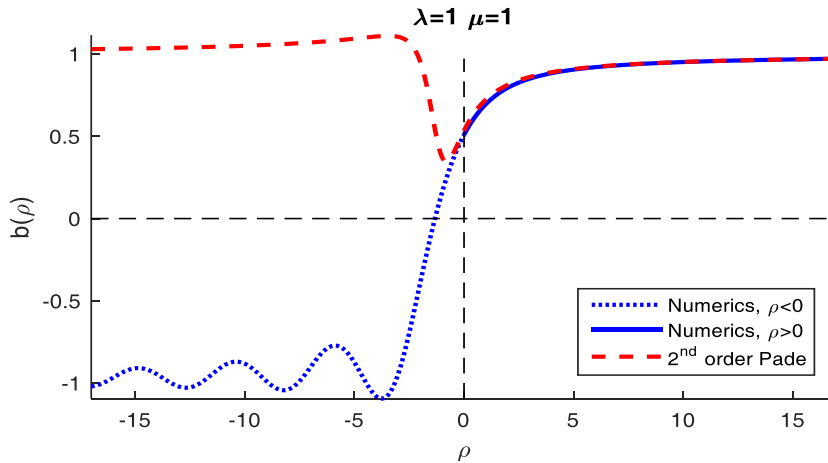


Figure 7. Comparison between the numerical solution (*blue solid and dotted curves*) and the 2nd order Padé approximation (*red dashed curve*, Eq.) for the dimensionless free buffer concentration at positive and negative (unphysical) values of distance, for $\lambda=\mu=1$. Despite the good agreement for physical distances ($\rho>0$), the analytic extension of true solution approaches $-\mu = -1$ as $\rho \rightarrow -\infty$, contrary to the rational function approximation, which always approaches +1 in this limit.

More importantly, it is possible that the presented approach can be extended to the study of complex buffers with more realistic Ca^{2+} binding properties. Although most of prior modeling efforts focused on a simple buffer with one-to-one Ca^{2+} binding stoichiometry, the case also considered here, most biological buffers possess several binding sites with distinct Ca^{2+} binding characteristics. If the binding to such multiple sites is independent (non-cooperative), they can be effectively modeled as a combination of several simple buffers with binding properties that correspond to each of the distinct binding sites. However, many widely expressed buffers such as calretinin and calmodulin are characterized by two-site molecular EF-hand domains with cooperative Ca^{2+} binding, whereby the binding of a second Ca^{2+} ion proceeds with much greater affinity once the first binding site is occupied, in a way similar to the oxygen binding to hemoglobin

(32, 45). In this case an additional small parameter corresponding to the ratio of affinities of the two Ca^{2+} -binding reactions would confound the asymptotic conditions of applicability of previously developed approximations. Because of the prominent role of calmodulin in a variety of Ca^{2+} -dependent pathways, including long-term potentiation (46), extending previously obtained results to cooperative buffering is important. Better tools for describing cooperative buffering may also help in interpreting imaging data obtained with the latest genetically encoded calmodulin-derived Ca^{2+} indicator dyes (47-50). More accurate description of binding dynamics of these dyes may help in increasing the temporal resolution of Ca^{2+} imaging obtained using these synthetic buffers. Our preliminary exploration suggests that obtaining the long-range (high- ρ) asymptotic series for the case of cooperative buffer is not significantly more complicated as compared to the simple-buffer case. Analysis of cooperative binding case will be investigated as a direct future extension of this work.

V. Acknowledgements

This work was supported by the National Science Foundation grant DMS-1517085

Appendix

In the case of non-zero background Ca^{2+} concentration infinitely far from channel, Ca^{2+} conservation condition, Eq. 5, reads

$$D_C(C - C_\infty) + D_B(B_\infty - B) = \frac{1}{4\pi F} \sum_{k=1}^N \frac{I_{Ca}}{|r - r_k|}, \quad (31)$$

where C_∞ and B_∞ are the background $[\text{Ca}^{2+}]$ and $[B]$ infinitely far from the channel and in equilibrium with each other: $B_\infty = B_T K_D / (K_D + C_\infty)$. Non-dimensionalizing this Ca^{2+} conservation condition for the case of a single channel at the origin, we obtain

$$c = c_\infty + v(b - b_\infty) + 1/\rho, \quad (32)$$

where the dimensionless background concentrations of buffer and Ca^{2+} , $b_\infty = B_\infty / B_T$ and $c_\infty = C_\infty / K_D$, are related by $b_\infty = 1/(1 + c_\infty)$. The dimensionless equation for free buffer then becomes (cf. Eq. 9):

$$\begin{cases} \text{Unbound buffer:} & \lambda \nabla_\rho^2 b = (b - b_\infty)(v b + b_\infty^{-1}) + b/\rho, \\ \text{Boundary conditions:} & \lim_{\rho \rightarrow 0} (\rho^2 b_\rho) = 0, \quad \lim_{\rho \rightarrow +\infty} b = b_\infty. \end{cases} \quad (33)$$

Asymptotic series for the solution near $x=0$ and the Taylor series near $\rho=0$ then read (cf. Eqs. 14,16):

$$\begin{cases} b(x) = b_\infty - \frac{b_\infty^2 x}{v b_\infty^2 + 1} + \left(\frac{b_\infty}{v b_\infty^2 + 1} \right)^3 x^2 + \frac{b_\infty^4 (v b_\infty^2 - 1)}{(v b_\infty^2 + 1)^5} x^3 + \left(\frac{b_\infty x}{v b_\infty^2 + 1} \right)^4 \left(2\lambda + \frac{b_\infty (v^2 b_\infty^4 - 3v b_\infty^2 + 1)}{(v b_\infty^2 + 1)^3} \right) + O(x^5), \\ b(\rho) = \sum_{n=0}^{\infty} b_n \rho^n = b_0 + \frac{b_0 \rho}{2\lambda} + \frac{(b - b_\infty)(v b_0 + b_\infty^{-1}) + b_0 / (2\lambda)}{6\lambda} \rho^2 + O(\rho^3). \end{cases} \quad (34)$$

Here $v=1/\mu$. The lowest-order Padé approximation is (cf. Eq. 18):

$$b\left(x = \frac{1}{\rho}\right) = B_\infty \frac{1 + A_1 x}{1 + B_1 x} = B_\infty \frac{\rho + A_1}{\rho + B_1}, \quad (35)$$

with coefficients given by (cf. Eq. 22):

$$A_1 = \frac{-b_\infty + [b_\infty (8\lambda (v b_\infty^2 + 1) + b_\infty)]^{1/2}}{2(1 + v b_\infty^2)}, \quad B_1 = \frac{b_\infty + [b_\infty (8\lambda (v b_\infty^2 + 1) + b_\infty)]^{1/2}}{2(1 + v b_\infty^2)}. \quad (36)$$

In dimensional forms, the Ca^{2+} and buffer concentrations corresponding to the lowest-order, bilinear approximation are given by

$$[\text{Buffer}] = B_\infty \frac{r + \hat{A}_1}{r + \hat{B}_1}, \quad [\text{Ca}^{2+}] = C_\infty + \frac{I_{Ca}}{4\pi D_C F r} + B_\infty \frac{D_B}{D_C} \frac{\hat{A}_1 - \hat{B}_1}{r + \hat{B}_1}. \quad (37)$$

where $\hat{A}_1 = A_1 I_{Ca} / (4\pi F K D_C)$, $\hat{B}_1 = B_1 I_{Ca} / (4\pi F K D_C)$, and F is the Faraday constant.

REFERENCES

1. Konieczny, V., M. V. Keebler, and C. W. Taylor. 2012. Spatial organization of intracellular Ca²⁺ signals. *Semin Cell Dev Biol* 23:172-180.
2. Thurley, K., A. Skupin, R. Thul, and M. Falcke. 2012. Fundamental properties of Ca²⁺ signals. *Biochim Biophys Acta* 1820:1185-1194.
3. Dupont, G., M. Falcke, V. Kirk, and J. Sneyd. 2016. *Models of Calcium Signalling*. Springer.
4. Oheim, M., F. Kirchhoff, and W. Stuhmer. 2006. Calcium microdomains in regulated exocytosis. *Cell Calcium* 40:423-439.
5. Berridge, M. J., P. Lipp, and M. D. Bootman. 2000. The versatility and universality of calcium signalling. *Nat Rev Mol Cell Biol* 1:11-21.
6. Augustine, G. J., F. Santamaria, and K. Tanaka. 2003. Local calcium signaling in neurons. *Neuron* 40:331-346.
7. Stanley, E. F. 2016. The Nanophysiology of Fast Transmitter Release. *Trends Neurosci* 39:183-197.
8. Matthews, E. A., and D. Dietrich. 2015. Buffer mobility and the regulation of neuronal calcium domains. *Front Cell Neurosci* 9:48.
9. Neher, E. 2000. Calcium buffers in flash-light. *Biophys J* 79:2783-2784.
10. Cheng, H., and W. J. Lederer. 2008. Calcium sparks. *Physiol Rev* 88:1491-1545.
11. Roberts, W. M. 1993. Spatial calcium buffering in saccular hair cells. *Nature* 363:74-76.
12. Simon, S. M., and R. R. Llinas. 1985. Compartmentalization of the submembrane calcium activity during calcium influx and its significance in transmitter release. *Biophys. J.* 48:485-498.
13. Fogelson, A. L., and R. S. Zucker. 1985. Presynaptic calcium diffusion from various arrays of single channels. Implications for transmitter release and synaptic facilitation. *Biophys. J.* 48:1003-1017.
14. Chad, J. E., and R. Eckert. 1984. Calcium domains associated with individual channels can account for anomalous voltage relations of CA-dependent responses. *Biophys J* 45:993-999.
15. Neher, E. 1998. Usefulness and limitations of linear approximations to the understanding of Ca⁺⁺ signals. *Cell Calcium* 24:345-357.
16. Aharon, S., H. Parnas, and I. Parnas. 1994. The magnitude and significance of Ca²⁺ domains for release of neurotransmitter. *Bull Math Biol* 56:1095-1119.
17. Smith, G. D., J. Wagner, and J. Keizer. 1996. Validity of the rapid buffering approximation near a point source of calcium ions. *Biophys J* 70:2527-2539.
18. Smith, G. D., L. X. Dai, R. M. Miura, and A. Sherman. 2001. Asymptotic analysis of buffered calcium diffusion near a point source. *Siam J Appl Math* 61:1816-1838.
19. Coggins, M., and D. Zenisek. 2009. Evidence that exocytosis is driven by calcium entry through multiple calcium channels in goldfish retinal bipolar cells. *J Neurophysiol* 101:2601-2619.
20. Nguyen, V., R. Mathias, and G. D. Smith. 2005. A stochastic automata network descriptor for Markov chain models of instantaneously coupled intracellular Ca²⁺ channels. *Bull Math Biol* 67:393-432.

21. Bertram, R., G. D. Smith, and A. Sherman. 1999. Modeling study of the effects of overlapping Ca²⁺ microdomains on neurotransmitter release. *Biophys J* 76:735-750.
22. Trommershauser, J., R. Schneggenburger, A. Zippelius, and E. Neher. 2003. Heterogeneous presynaptic release probabilities: functional relevance for short-term plasticity. *Biophys J* 84:1563-1579.
23. Pape, P. C., D. S. Jong, and W. K. Chandler. 1995. Calcium release and its voltage dependence in frog cut muscle fibers equilibrated with 20 mM EGTA. *J Gen Physiol* 106:259-336.
24. Rudiger, S., J. W. Shuai, W. Huisinga, C. Nagaiah, G. Warnecke, I. Parker, and M. Falcke. 2007. Hybrid stochastic and deterministic simulations of calcium blips. *Biophys J* 93:1847-1857.
25. Weinberg, S. H., and G. D. Smith. 2014. The influence of Ca²⁺(+) buffers on free [Ca²⁺(+)] fluctuations and the effective volume of Ca²⁺(+) microdomains. *Biophys J* 106:2693-2709.
26. Wieder, N., R. Fink, and F. von Wegner. 2015. Exact stochastic simulation of a calcium microdomain reveals the impact of Ca²⁺(+) fluctuations on IP₃R gating. *Biophys J* 108:557-567.
27. Neher, E. 1986. Concentration profiles of intracellular Ca²⁺ in the presence of diffusible chelator. In *Calcium Electrogenesis and Neuronal Functioning*. U. Heinemann, M. Klee, E. Neher, W. Singer, editor. Springer-Verlag. 80-96.
28. Neher, E., and G. J. Augustine. 1992. Calcium gradients and buffers in bovine chromaffin cells. *J Physiol* 450:273-301.
29. Wagner, J., and J. Keizer. 1994. Effects of rapid buffers on Ca²⁺ diffusion and Ca²⁺ oscillations. *Biophys J* 67:447-456.
30. Stern, M. D. 1992. Buffering of calcium in the vicinity of a channel pore. *Cell Calcium* 13:183-192.
31. Naraghi, M., and E. Neher. 1997. Linearized buffered Ca²⁺ diffusion in microdomains and its implications for calculation of [Ca²⁺] at the mouth of a calcium channel. *J Neurosci* 17:6961-6973.
32. Schwaller, B. 2009. The continuing disappearance of "pure" Ca²⁺ buffers. *Cell Mol Life Sci* 66:275-300.
33. Falcke, M. 2003. On the role of stochastic channel behavior in intracellular Ca²⁺ dynamics. *Biophys J* 84:42-56.
34. Falcke, M. 2003. Buffers and oscillations in intracellular Ca²⁺ dynamics. *Biophys J* 84:28-41.
35. Naraghi, M. 1997. T-jump study of calcium binding kinetics of calcium chelators. *Cell Calcium* 22:255-268.
36. Lee, S. H., B. Schwaller, and E. Neher. 2000. Kinetics of Ca²⁺ binding to parvalbumin in bovine chromaffin cells: implications for [Ca²⁺] transients of neuronal dendrites. *J Physiol* 525 Pt 2:419-432.
37. Schmidt, H., E. B. Brown, B. Schwaller, and J. Eilers. 2003. Diffusional mobility of parvalbumin in spiny dendrites of cerebellar purkinje neurons quantified by fluorescence recovery after photobleaching. *Biophys J* 84:2599-2608.
38. Schmidt, H., O. Arendt, E. B. Brown, B. Schwaller, and J. Eilers. 2007. Parvalbumin is freely mobile in axons, somata and nuclei of cerebellar Purkinje neurones. *J Neurochem* 100:727-735.
39. Baylor, S. M., and S. Hollingworth. 1998. Model of sarcomeric Ca²⁺ movements, including ATP Ca²⁺ binding and diffusion, during activation of frog skeletal muscle. *J Gen Physiol* 112:297-316.

40. Allbritton, N. L., T. Meyer, and L. Stryer. 1992. Range of messenger action of calcium ion and inositol 1,4,5-trisphosphate. *Science* 258:1812-1815.
41. Smith, G. D. 1996. Analytical steady-state solution to the rapid buffering approximation near an open Ca²⁺ channel. *Biophys J* 71:3064-3072.
42. Thul, R., and M. Falcke. 2004. Release currents of IP(3) receptor channel clusters and concentration profiles. *Biophys J* 86:2660-2673.
43. Bentele, K., and M. Falcke. 2007. Quasi-steady approximation for ion channel currents. *Biophys J* 93:2597-2608.
44. Zucker, R. S., and A. L. Fogelson. 1986. Relationship between transmitter release and presynaptic calcium influx when calcium enters through discrete channels. *Proc Natl Acad Sci U S A* 83:3032-3036.
45. Schwaller, B. 2014. Calretinin: from a "simple" Ca(2+) buffer to a multifunctional protein implicated in many biological processes. *Front Neuroanat* 8:3.
46. Raghuram, V., Y. Sharma, and M. R. Kreutz. 2012. Ca(2+) sensor proteins in dendritic spines: a race for Ca(2+). *Front Mol Neurosci* 5:61.
47. Wilms, C. D., and M. Hausser. 2009. Lighting up neural networks using a new generation of genetically encoded calcium sensors. *Nat Methods* 6:871-872.
48. Dreosti, E., B. Odermatt, M. M. Dorostkar, and L. Lagnado. 2009. A genetically encoded reporter of synaptic activity in vivo. *Nat Methods* 6:883-889.
49. Helassa, N., X. H. Zhang, I. Conte, J. Scaringi, E. Esposito, J. Bradley, T. Carter, D. Ogden, M. Morad, and K. Torok. 2015. Fast-Response Calmodulin-Based Fluorescent Indicators Reveal Rapid Intracellular Calcium Dynamics. *Sci Rep* 5:15978.
50. Chen, T. W., T. J. Wardill, Y. Sun, S. R. Pulver, S. L. Renninger, A. Baohan, E. R. Schreiter, R. A. Kerr, M. B. Orger, V. Jayaraman, L. L. Looger, K. Svoboda, and D. S. Kim. 2013. Ultrasensitive fluorescent proteins for imaging neuronal activity. *Nature* 499:295-300.